

Efficient Interactive 3D Multi-Object Removal

Jingcheng Ni^{1,2*}, Weiguang Zhao^{4,5*}, Daniel Wang³, Ziyao Zeng³,
Chenyu You⁶, Alex Wong³, Kaizhu Huang^{1†}

¹Duke Kunshan University, ²Duke University, ³Yale University,
⁴Xi'an Jiaotong-Liverpool University, ⁵University of Liverpool, ⁶Stony Brook University
{jingcheng.ni, kaizhu.huang}@dukekunshan.edu.cn, weiguang.zhao@liverpool.ac.uk

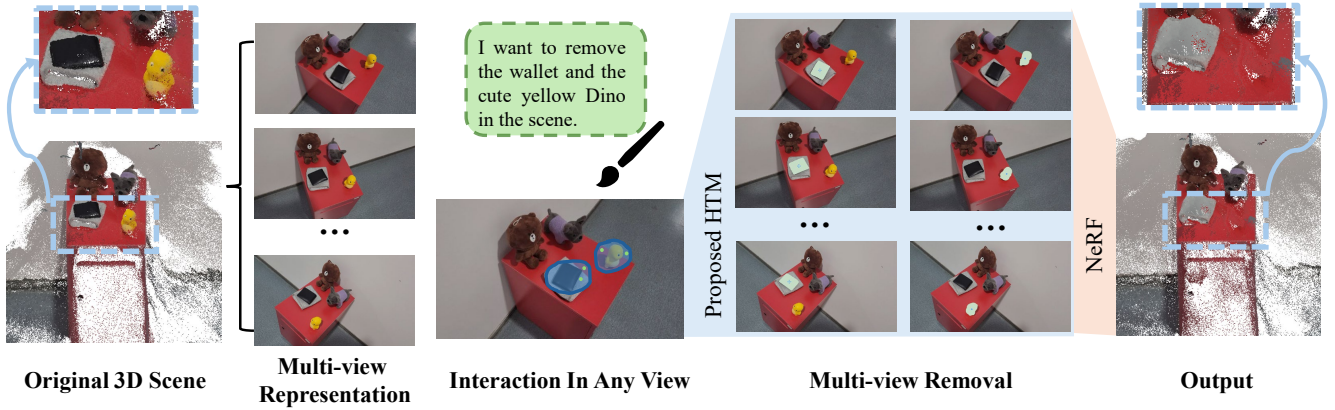


Figure 1: Efficient Interactive 3D Multi-Object Removal. The blue shaded area represents the selected removal area. The red dot stands for the selected background and the objects to be retained. HTM is Homography-based Masks Matching Module.

Abstract

Object removal is of great significance to 3D scene understanding, essential for applications in content filtering and scene editing. Current mainstream methods primarily focus on removing individual objects, with a few methods dedicated to eliminating an entire area or all objects of a certain category. They however confront the challenge of insufficient granularity and flexibility for real-world applications, where users demand tailored excision and preservation of objects within defined zones. In addition, most of the current methods require kinds of priors when addressing multi-view inpainting, which is time-consuming. To address these limitations, we propose an efficient and user-friendly pipeline for 3D multi-object removal, enabling users to flexibly select areas and define objects for removal or preservation. Concretely, to ensure object consistency and correspondence across multiple views, we propose a novel mask matching and refinement module, which integrates homography-based warping with high-confidence anchor points for segmentation. By leveraging the IoU joint shape context distance

loss, we enhance the accuracy of warped masks and improve subsequent inpainting processes. Considering the current immaturity of 3D multi-object removal, we provide a new evaluation dataset to bridge the developmental void. Experimental results demonstrate that our method significantly reduces computational costs, achieving processing speeds more than 80% faster than state-of-the-art methods while maintaining equivalent or higher reconstruction quality.

1 Introduction

3D object removal refers to the process of eliminating specified entities from the 3D scene and completing the visual gap caused by the removal. The application of 3D object removal techniques offers significant benefits, including the enhancement of scene understanding and data integrity by eliminating unwanted or erroneous objects from 3D representations. This process facilitates more accurate and reliable downstream tasks such as object recognition, scene reconstruction, and robotic navigation, thereby improving overall system performance.

Recent advances in 3D objects removal [Mirzaei *et al.*, 2023b; Weder *et al.*, 2023; Mirzaei *et al.*, 2023a; Chen *et al.*, 2024; Wei *et al.*, 2023; Wang *et al.*, 2024a] have demonstrated significant achievements. However, several critical

*Equal contribution.

†Corresponding author.

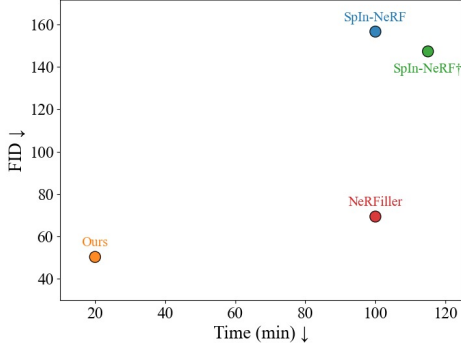


Figure 2: Efficiency and FID comparisons for different models. SPIn-NeRF[†] stands for SPIn-NeRF with refined RGB

challenges still remain, particularly concerning the complexity and efficiency of object-selecting methods and removing procedures, multi-object handling, and the reliance on precise depth information and camera poses. The current approaches for object specification in removal tasks are complex and inefficient, especially in scenes containing multiple objects. Some methods require users to identify objects by selecting representative points, a process that becomes increasingly time-consuming with multiple objects and often fails to ensure comprehensive object representation. Alternative approaches focusing on object selection within 3D representations, such as point clouds or meshes, demand substantial technical expertise from users while being both time-intensive and prone to accuracy issues. Another significant limitation of existing methods lies in their primary focus on single-object removal, which proves insufficient for many real-world applications. In multi-object scenarios, these methods struggle to maintain consistent object correspondence across different views. For instance, when a user selects multiple objects from one particular NeRF-rendered viewpoint, current methods often fail to accurately identify the corresponding objects from alternative perspectives.

The reliance on accurate depth maps and camera poses for visual gap filling in NeRF scenes presents another substantial challenge. While existing methods have shown promising results, most of them heavily depend on depth information, RGB priors, and camera parameters (e.g. intrinsic and extrinsic pose matrices), in order to assist with mask localization and removal processes. This dependency creates critical complications in practical applications. First, obtaining depth or RGB priors often requires additional NeRF training, which significantly increases its computational costs. Second, the accuracy of depth information is intrinsically tied to the quality of NeRF training, yet the input images used for training may be of suboptimal quality, leading to unreliable estimates. Third, the camera poses used in these systems frequently contain estimation errors, which could propagate through the entire pipeline and thus affect the final results.

To tackle these challenges, as illustrated in Fig. 1, we propose an intuitive and interactive multi-object removal framework. Users begin by selecting any single view, outlining

the region containing the target objects for removal, and then clicking to specify objects to retain. The process culminates in providing a refined 3D scene with the selected objects removed. This approach is particularly effective for scenarios requiring the removal of multiple objects. In addition, our method introduces an innovative multi-view multi-object matching pipeline comprising two key components: mask mapping and anchor point adaptive adjustment.

Our method leverages a pre-trained LoFTR to establish keypoint correspondences across multiple views. Based on these matched keypoints, we compute homography matrices to map object masks from the interaction view to other multi-view images. Furthermore, we construct an anchor point circle centered on the mapped mask’s centroid, sampling points along this circle as point prompts for SAM2 [Kirillov *et al.*, 2023; Ravi *et al.*, 2024] in the respective view. We introduce gradient optimization to adaptively adjust these point prompts, utilizing IoU (Intersection over Union) and shape distance constraints as references to optimize the anchor circle’s dimensions. This approach enables us to identify corresponding regions across multi-view images without requiring depth data or multi-view pose information, significantly enhancing practical applicability and efficiency.

Our method further leverages region correspondences across all viewpoints to facilitate subsequent mask region completion. We select key viewpoints and employ the LaMa model to complete regions marked for removal, then utilize previously computed homography matrices to map the completed regions to adjacent viewpoints. In this way, we not only enhance multi-view consistency but also substantially reduce the overall processing time from several hours to approximately 20 minutes as shown in Fig. 2.

Additionally, we address the limitation of existing 3D multi-view removal datasets [Mirzaei *et al.*, 2023b; Weber *et al.*, 2024], which lack diverse object samples necessary for tackling multi-object removal challenges. In this regard, we introduce a comprehensive 3D multi-object multi-view removal dataset composed of real-world scenes. Extensive experimentation validates the effectiveness of our approach, demonstrating its practicality in real-world open scenarios. Our method achieves state-of-the-art performance on both public datasets and our proposed dataset. The contributions of our work are as follows:

- We develop a more user-friendly interaction approach for 3D multi-object removal, which allows users to select arbitrary-shaped regions and then mark on areas or objects to be retained. This method enhances the flexibility the removal task.
- We propose a novel adaptive anchor-based multi-object matching module that accurately constructs the indexing of corresponding object masks across multiple views, ensuring consistency in 3D multi-view object removal.
- We design a warping-based joint inpainting algorithm. By leveraging homography matrix-based warping, we significantly reduce inpainting costs, shorten multi-view inpainting time, and enhance overall efficiency.
- Our proposed method achieves state-of-the-art performance on existing datasets and our dataset. Moreover,

it does not require any additional precise depth, poses, and training, enabling its direct application to real-world open scenes.

2 Related Work

2.1 Multi-View 3D Scene Understanding

Methods for 3D scene understanding can typically be divided into three categories [Guo *et al.*, 2020]: point-based methods [Qi *et al.*, 2017a; Qi *et al.*, 2017b; Wu *et al.*, 2022; Wu *et al.*, 2024; Zhang *et al.*, 2021; Zhu *et al.*, 2023a], voxel-based methods [Maturana and Scherer, 2015; Choy *et al.*, 2019; Zhao *et al.*, 2023], and multi-view methods [Hu *et al.*, 2021; Yang *et al.*, 2023]. The rapid development of visual language models [Radford *et al.*, 2021; Rombach *et al.*, 2022; Yang *et al.*, 2024a; Yang *et al.*, 2024b] and visual foundation models [Vaswani *et al.*, 2017; Dosovitskiy, 2020; Gu and Dao, 2023] has empowered a useful foundation for downstream tasks [Chen *et al.*, 2023; Zhang *et al.*, 2022b; Zeng *et al.*, 2024b; Zeng *et al.*, 2024c], particularly leading to a surge in methods that render 3D objects into 2D multi-view images for feature extraction or prediction. Specifically, some methods [Zhang *et al.*, 2022a; Zhu *et al.*, 2023b; Shen *et al.*, 2024; Zhao *et al.*, 2025] project the 3D object into multi-view images and leverage the CLIP [Radford *et al.*, 2021] or Diffusion [Rombach *et al.*, 2022; Ho *et al.*, 2020; Zeng *et al.*, 2024a] to get the final recognition result. Moreover, methods [Genova *et al.*, 2021; Hu *et al.*, 2021; Yang *et al.*, 2023] extract the multi-view images from videos of 3D scene and utilize the 2D network to achieve the segmentation prediction. In light of this, our work combines the multi-view images and pre-trained 2D visual models [Sun *et al.*, 2021; Suvorov *et al.*, 2022] to attain the 3D scene removal without training labels.

2.2 Object Removal in 2D Domain

Most 2D object removal approaches [Avrahami *et al.*, 2023; Avrahami *et al.*, 2022; Lugmayr *et al.*, 2022; Nichol *et al.*, 2021; Xie *et al.*, 2023] erase the objects from RGB images/videos and engage the diffusion model [Rombach *et al.*, 2022; Ho *et al.*, 2020] to inpaint the erased images/videos. Several more challenging and highly relevant tasks are currently being explored, including large hole filling [Li *et al.*, 2022; Suvorov *et al.*, 2022] and pluralistic inpainting [Zheng *et al.*, 2019; Wan *et al.*, 2021]. Moreover, Context-Encoders [Pathak *et al.*, 2016] combine adversarial training with the encoder-decoder structure into this task. Furthermore, recurrent [Li *et al.*, 2020; Zhang *et al.*, 2018], gated convolution [Yu *et al.*, 2019] and multi-stage [Ren *et al.*, 2019] methods are proposed to enhance the effectiveness of object removal. More recent advancements, such as LaMa [Suvorov *et al.*, 2022], are designed to tackle the challenges associated with large missing regions and high-resolution images. Specifically, LaMa leverages fast Fourier convolutions to effectively capture global context from the initial stages of processing and incorporates a high receptive field perceptual loss and a strategic approach to mask generation during training. Since our goal is to blend the inpainted area with the surrounding background without the necessity

of text prompts, our pipeline employs LaMa, which is better suited for achieving the desired level of coherence in object removal tasks.

2.3 Object Removal in 3D Domain

Current works [Mirzaei *et al.*, 2023b; Weder *et al.*, 2023; Mirzaei *et al.*, 2023a; Chen *et al.*, 2024; Lu *et al.*, 2024] on 3D object removal mainly focus on alleviating inconsistencies in NeRF scene inpainting. Specifically, Remove-NeRF [Weder *et al.*, 2023] lightens the inconsistencies using the inpainting confidence based view selection procedure. Moreover, SPIn-NeRF [Mirzaei *et al.*, 2023b] and In-NeRF360 [Wang *et al.*, 2024a] employ the perceptual loss within inpainted regions to reduce inconsistencies between different views. Additionally, GScream [Wang *et al.*, 2024b] introduces Gaussian splatting as a method to bolster geometric consistency across the edited scenes. Furthermore, NeR-Filler [Weber *et al.*, 2024] focuses on completing scenes and leverages an iterative framework that utilizes the 2×2 grid behavior of 2D inpainting models to 3D consistency. In addition, Clutter-DR [Wei *et al.*, 2023] employs 3D segmentation alongside instance-level area-sensitive losses to enhance the clarity and visual appeal of the inpainted scenes.

Although these methods have achieved certain improvements in this task, they still show some weaknesses in practical multi-object removal. First, the interaction for determining the objects to be removed in these methods is unfriendly and laborious. SOTAs [Mirzaei *et al.*, 2023b; Weder *et al.*, 2023; Mirzaei *et al.*, 2023a; Chen *et al.*, 2024; Lin *et al.*, 2024] require multiple interactions or iterative interactions to achieve multi-object removal. Meanwhile, Clutter-DR [Wei *et al.*, 2023] directly removes all objects of predefined categories in all 3D scenes. In contrast, our method offers a more friendly pipeline to remove multiple objects within one single interaction. Furthermore, SOTAs [Mirzaei *et al.*, 2023b; Weder *et al.*, 2023] demonstrate low efficiency in multi-view mask generation and matching. Especially, Remove-NeRF [Weder *et al.*, 2023] involves manually annotating a 3D box around the object using MeshLab, which is also complex and time-consuming for users. On the contrary, our method simplifies this process and enables the easy generation and matching of well-formed multi-view masks.

3 Proposed Method

3.1 Overview

Fig. 3 overviews our proposed method which mainly consists of the following three parts: Interaction Processing (a), Multi-View Objects Removal (b), and 3D Reconstruction (c). Following recent SOTAs [Wei *et al.*, 2023; Mirzaei *et al.*, 2023a; Chen *et al.*, 2024], multi-view images are adopted as the network input. Note that these multi-view images could reconstruct the 3D scene that needs to be cleaned up. First, we select any image from the input that we want to interact with, and then outline the interactive area and the objects to be retained. The pre-trained SAM2 [Kirillov *et al.*, 2023; Ravi *et al.*, 2024] is used to segment the interactive view image to obtain the binary mask of the object to be removed.

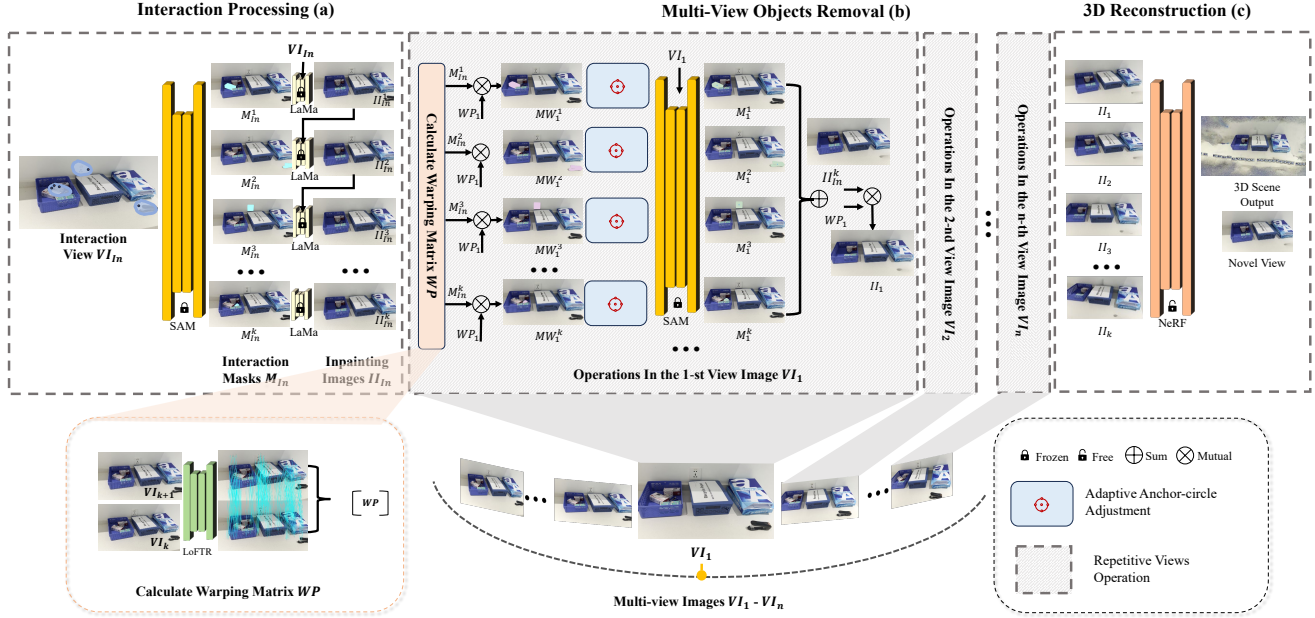


Figure 3: Network Architecture.

Subsequently, we utilize LaMa [Suvorov *et al.*, 2022] in combination with the binary mask to sequentially inpaint the interactive view image. Furthermore, we leverage LoFTR [Sun *et al.*, 2021] to generate keypoint correspondences between adjacent view images to compute their homography matrix for warping. Moreover, leveraging the warping matrix, we design the adaptive anchor-circle adjustment algorithm to generate SAM2 point prompts for each view. This process enables us to obtain binary masks for the objects to be removed in each view. Additionally, we utilize the warping matrices between adjacent view images and the LaMa model to sequentially inpaint multi-view images where objects have been removed. Finally, the inpainted multi-view images and poses act as inputs for training the NeRF and reconstructing the 3D scene.

3.2 Interaction Processing

Interaction. Different from many current SOTAs [Mirzaei *et al.*, 2023b; Weder *et al.*, 2023; Mirzaei *et al.*, 2023a; Chen *et al.*, 2024], we develop a novel interactive method for 3D scene removal, more concise and versatile. In this regard, users can interactively select arbitrary regions which cover unwanted objects and remain the desired objects by marking on them in any view. These regions may contain unwanted objects, yet the desired objects can be preserved by the user. As shown in Fig. 1, our interaction operation mainly includes two steps: 1) Mark one removal area, and 2) Click background & remaining objects. Specifically, we first mark out the areas to be removed in the selected interactive view, and then click on the background of the current area, such as the desktop or floor. Furthermore, if there are objects that need to be retained, we also click on them. This interactive information will serve as a crucial inference information for

our 3D multi-object removal.

Segmentation and Inpainting of Interaction View. Given an interactive view image VI_{In} , we input it into SAM2 to obtain binary interaction masks $M_{In} = \{M_{In}^i \in \mathbb{R}^{W \times H \times 1}\}_{i=1}^K$ for the K objects to be removed, where M_{In}^i denotes the i_{th} binary interaction masks, W and H stands for the width and height of the image, respectively. The masks M_{In} contain only 0 and 1 values, where 0 indicates the retained parts and 1 represents the parts to be removed. As shown in Fig. 3, using these binary masks M_{In} and a pre-trained LaMa model, we sequentially remove K objects for the interactive image VI_{In} and perform inpainting.

Specifically, we apply the binary mask M_{In}^1 of the first object to be removed to zero out the corresponding RGB values in image VI_{In} . Then, we employ LaMa to inpaint the image and obtain the image II_{in}^1 as follows:

$$II_{in}^1 = LaMa(M_{In}^1 \cdot VI_{In}). \quad (1)$$

Furthermore, we apply the binary mask M_{In}^2 of the second object to be removed to zero out the corresponding RGB values in image II_{in}^1 . Then, we take LaMa to inpaint the image and obtain the image II_{in}^2 with both the first and second objects removed. By extending this process, the interactive view image II_{in}^K with all K objects removed can be obtained as below:

$$II_{in}^K = LaMa(M_{In}^{K-1} \cdot II_{in}^{K-1}), K > 1. \quad (2)$$

Both M_{In} and II_{in}^K serve as the significant inference information for our multi-view images object removal.

3.3 Multi-View Object Removal

Given one set multi-view images $VI = \{VI_j \in \mathbb{R}^{W \times H \times 3}\}_{j=1}^{N_v}$, where VI_j denotes the j_{th} view image and

N_v implies the number of all views. Our method primarily relies on the keypoint correspondences and mask mappings between multi-view images to achieve object removal. Traditional pairwise mapping would result in $N_v \cdot (N_v + 1)$ pairs, leading to significant memory and time overhead. We propose using LoFTR [Sun *et al.*, 2021] to measure viewpoint similarity. By only considering adjacent views for object removal, we reduce the number of pairs to N , thus significantly lowering the computational requirements.

Since the operations for each view are iteratively identical, with the mask M_{In} and image I_{In} from the previous view serving as the matching information for the next view. For simplicity, we will detail the process for one view only as shown in Fig. 3. The operations for each view consist of two main parts: 1) computing the warping matrix using keypoints between two views, and 2) generating adaptive anchor circles using the warped mask to sample point prompts for SAM2. We detail these two operations in the following subsections.

Homography Matrix for Mask Warping. Homography matrix represents a projective transformation between two planes. In the context of planar surfaces, this transformation can be represented by a 3x3 matrix H that maps points from one plane to another while preserving collinearity and cross-ratio properties. Given a point in homogeneous coordinates, the homography transformation can be expressed as:

$$\begin{bmatrix} x' \\ y' \\ w' \end{bmatrix} = \begin{bmatrix} h_{11} & h_{12} & h_{13} \\ h_{21} & h_{22} & h_{23} \\ h_{31} & h_{32} & h_{33} \end{bmatrix} \begin{bmatrix} x \\ y \\ 1 \end{bmatrix}.$$

Each matched point pair (p_i, p'_i) provides two constraint equations for computing the homography matrix. While theoretically four point correspondences are sufficient to determine the homography matrix due to its eight degrees of freedom, utilizing just four points would be susceptible to noise and matching errors. We iteratively samples minimal sets of four correspondences to compute candidate homography matrices. For each iteration, a candidate matrix is computed and evaluated against all matching points using the reprojection error:

$$\varepsilon = \sum_{i=1}^n \|p'_i - H \cdot p_i\|^2.$$

This identifies inliers (points with error below a threshold) and selects the homography matrix that maximizes the number of inliers, which helps find an optimal solution that best fits the majority of correspondences.

Given a binary mask M_i at view i and the computed homography matrix $H_{i,i+1}$ between consecutive images i and $i + 1$, the warping process transforms M_i to align with image $i + 1$, resulting in the warped mask MW_{i+1} . For each pixel position in the target image, we compute its corresponding position in the source image using the inverse homography transformation:

$$MW_{i+1}(x, y) = MW_i(H_{i,i+1}^{-1} \begin{bmatrix} x \\ y \\ 1 \end{bmatrix}).$$

This transformation maintains the topology of the mask region while adjusting its geometric shape according to the perspective change between multi-view images.

Adaptive Anchor-circle Adjustment. Through the homography matrices, we can obtain the warping mask $MW_i^k, MW_i^k \in \mathbb{R}^{W \times H}$ for the k -th object to be removed in the i -th view. The center point C_i^k of the warping mask MW_i^k serves as the initial center of the anchor circle with initial radius r . We sample points from the initial anchor circle to serve as the SAM2 point prompts for the i -th view image VI_i . Furthermore, we combine the point prompts and VI_i as the input of SAM2 to achieve the initial object mask M_i^k . We treat r as an optimization variable for gradient descent and use the IoU and Shape Context Distance between M_i^k and MW_i^k as the optimization constraint. The IoU metric ensures overall mask alignment, while the Shape Context Distance captures fine-grained shape similarities. This dual-constraint optimization can be formulated as:

$$\mathcal{L} = \alpha(1 - \text{IoU}(M_i^k, MW_i^k)) + \beta \cdot \text{SC}(M_i^k, MW_i^k), \quad (3)$$

where $\text{SC}(\cdot)$ represents the Shape Context Distance between two masks, and α, β are weighting coefficients balancing the contribution of each term. We iteratively find the optimal value of r by maximizing the equation.

3.4 3D Reconstruction

We utilize NeRF [Mildenhall *et al.*, 2021] to refine the multi-view consistency of inpainting results and reconstruct the 3D scene. NeRF models a scene by learning a mapping from 3D coordinates and views directions to color and density using one multi-layer perceptron (MLP), F_θ . For a given ray r , the estimated color $\hat{C}(r)$ is computed via volumetric rendering:

$$\hat{C}(r) = \sum_{i=1}^K T_i(1 - \exp(-\sigma_i \delta_i))c_i, \quad (4)$$

where c_i and σ_i are the color and density at the i -th sample along the ray, $\delta_i = t_{i+1} - t_i$ represents the distance between consecutive samples, and $T_i = \exp\left(-\sum_{j=1}^{i-1} \sigma_j \delta_j\right)$ represents the accumulated transmittance along the ray.

The model is trained by minimizing the loss between the rendered images and the ground-truth images from the training set, expressed as:

$$L = \sum_{r \in \mathcal{R}} \|\hat{C}(r) - C_{GT}(r)\|^2, \quad (5)$$

where \mathcal{R} is a batch of rays sampled from the training views, and $C_{GT}(r)$ denotes the ground-truth color for ray r .

3.5 Stability Augmentation

Considering the various complex scenes in the open world, we highlight here several detailed refinements aimed at improving model stability in real applications.

Inpainting. As described in Section 3.2, our image inpainting can be performed in two main ways: sequentially inpainting each mask, or inpainting all masks at once after merging them. We provide specific implementations for both approaches, which can be selected based on the actual application scenario. The sequential inpainting method is generally suitable for situations with many objects and uniform colors,

while the single-step inpainting method is more appropriate for scenarios with richer colors or time constraints.

Occlusion. Our proposed method is based on adjacent view object anchors. If the target object disappears in one of the intermediate views, it can cause the object to be lost in all subsequent views. To address this, we optimize the implementation by realigning with the interactive view and performing inpainting every 10 adjacent views rather than continuing to use the previous adjacent views.

4 Experiments

4.1 Experiment Setting

Datasets. We validate the effectiveness and applicability of our method on two datasets: the SPIn-NeRF dataset [Mirzaei *et al.*, 2023b] and our proposed multi-object open scenes dataset. The SPIn-NeRF dataset is currently one of the most popular datasets and used by state-of-the-art methods. It includes ground truth for scenes after object removal. However, it contains only 10 scenes, each with approximately 1 to 3 objects, and focuses on the removal of a single masked object per scene. In contrast, our proposed multi-object open scenes dataset comprises 30 scenes, each featuring more than five removable objects. Furthermore, our dataset introduces greater variation in viewpoints, making it more complex and better suited for real-world scenarios.

Evaluation Metrics. Following relevant recent works [Mirzaei *et al.*, 2023b; Wang *et al.*, 2024a; Weber *et al.*, 2024], we adapt standardized metrics PSNR, SSIM and LPIPS to evaluate the quality of the rendered images after object removal. In addition, we measure the efficiency of the methods in terms of runtime. We also report the Fréchet Inception Distance (FID) to assess the perceptual similarity between the rendered images and the ground truth. Additionally, for our dataset, we evaluate the average time for the model to train from start to convergence, including the inpainting process.

Experimental Setup. We conduct all evaluations on a single NVIDIA GeForce RTX 3090 GPU with 24GB VRAM. The implementation leverages Nerfstudio [Tancik *et al.*, 2023] as the foundational framework for training both our proposed method and NeRFiller. To obtain camera poses and intrinsic parameters for our dataset, we employed COLMAP [Schönberger *et al.*, 2016].

4.2 Results

Multiview Masks Matching. Our dataset is mainly used to evaluate the multiview masks matching. Since NeRFiller does not directly provide masks, we employ two approaches to generate them. Following SPIn-NeRF, we select points on each object to be removed in the first frame and utilize the SAM2 model to generate the corresponding masks. These masks are then used as initialization for DINO, which subsequently generates masks for the remaining frames. Our approach involves user interaction to create a mask in any chosen viewpoint. Through our mask matching module, we propagate the mask to corresponding masks across all other viewpoints. These two sets of masks are then provided to NeRFiller, producing the results shown in Tab. 1 and Image

1. As demonstrated, our masks are better in multiview masks matching accuracy and efficiency.

As shown in Fig. 5, the mask quality obtained through SPIn-NeRF is significantly inferior to our proposed method. Our analysis reveals two primary factors contributing to this quality disparity. First, SPIn-NeRF’s point-based selection approach often results in incomplete object coverage during the initial selection phase, leading to partial object omission. Second, when DINO generates masks for alternative viewpoints, it introduces substantial distortions to the object’s shape and boundaries. Furthermore, the mask propagation process in DINO exhibits inherent tracking instability, potentially leading to incomplete object removal outcomes.

Methods	PSNR \uparrow	SSIM \downarrow	LPIPS \downarrow
NeRFiller + SPIn-NeRF	27.42	0.85	0.14
NeRFiller + Ours	30.38	0.86	0.11

Table 1: Evaluation on Our Dataset

Multiview Inpainting. The SPIn-NeRF dataset with ground truth is utilized to evaluate the quality and consistency of multiview inpainting. For SPIn-NeRF, we directly use the values reported in the paper [Mirzaei *et al.*, 2023b]. For NeRFiller, we follow the instructions provided in the paper to use reference inpainting, rendering the test view images for comparison with the ground truth. For our proposed method, we employ two approaches: (1) utilizing the precise masks provided by SPIn-NeRF to perform warping joint inpainting, and (2) using only the mask from the first view and applying our multiview mask matching method to generate the masks for the remaining views. Similarly, our method renders images from test views and compares them with the ground truth to calculate LPIPS and FID metrics. As shown in Tab. 2 and Fig. 6, our method achieves LPIPS comparable to the other two methods while significantly outperforming them in terms of FID.

Methods	LPIPS \downarrow	FID \downarrow
SPIn-NeRF	0.47	156.64
SPIn-NeRF [†]	0.46	147.31
NeRFiller	0.53	69.40
Ours(with first mask)	0.56	50.35
Ours	0.52	51.78

Table 2: Evaluation on SPIn-NeRF Dataset. SPIn-NeRF[†] stands for SPIn-NeRF with refined RGB.

Efficiency. The comparative evaluation of interaction time and removal time highlights the efficiency of our method in

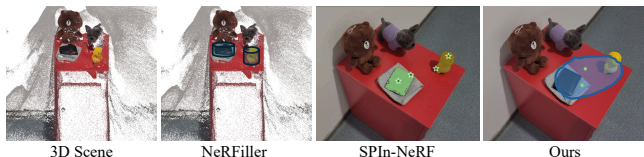


Figure 4: Interaction Comparison



Figure 5: **NeRF renderings for our dataset.** w stands for *with*. We show the rendering of the first test pose for 4 sampled scenes in our dataset. We compare our method to the NeRFiller results using DINO masks, as well as using our generated masks on the second row, and our method on the third row.

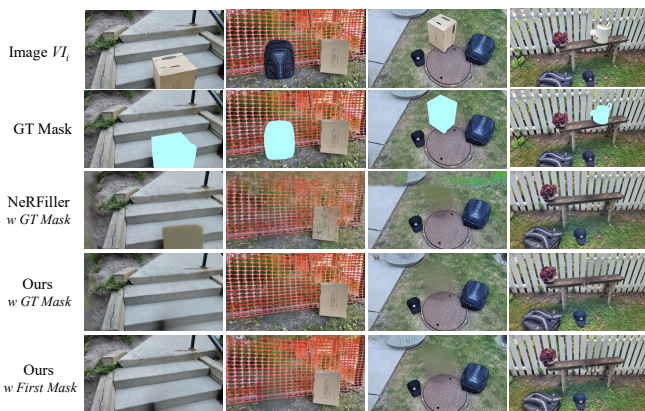


Figure 6: **NeRF renderings for SPIn-NeRF dataset.** w stands for *with* and GT donates ground-truth. We show the rendering of the first test pose for 4 sampled scenes in the SPIn-NeRF dataset. We compare our method to the NeRFiller results using ground truth masks, as well as using our generated masks on the third row.

handling multi-object scenarios. As shown in Fig. 4 and Tab. 3, our method offers more usability through its streamlined and intuitive interface. When handling two objects simultaneously, our approach requires only 3.4 seconds, representing a 24.4% improvement over SPIn-NeRF and a 94.3% reduction compared to NeRFiller. This efficiency gap widens further in three-object scenarios, where our method completes processing in 3.6 seconds, achieving a 29.4% improvement over SPIn-NeRF and a 96.0% reduction compared to NeRFiller. In addition, Our method maintains near-constant time complexity with increasing object count. The processing time increases by only 0.4 seconds when moving from one to two objects, and by 0.2 seconds when advancing to three objects. In contrast, other methods show obvious increases in interaction time as the number of objects grows.

The removal time metric further underscores our method’s efficiency, requiring only 20 minutes compared to 100 minutes for SPIn-NeRF and NeRFiller, and 115 minutes for SPIn-NeRF with refined RGB. This represents an 80% reduction

in removal time versus the standard implementations and an 82.6% improvement over SPIn-NeRF with refined RGB.

These results demonstrate that our method not only achieves faster processing times but also maintains consistent performance across varying levels of scene complexity. Such characteristics make our approach particularly suitable for real-world applications where complex, multi-object scenes are common.

Methods	Interaction Time ↓			Removal Time ↓
	One Obj.	Two Obj.	Three Obj.	
SPIn-NeRF	3.1 s	4.5 s	5.1 s	100.0 m
SPIn-NeRF [†]	3.1 s	4.5 s	5.1 s	115.0 m
NeRFiller	5.0 m	10.0 m	15.0 m	100.0 m
Ours	3.0 s	3.4 s	3.6 s	20.0 m

Table 3: Comparison on the Time Cost. Obj. stands for the objects. s stands for seconds and m stands for minute.

5 Conclusion

In this paper, we introduce a novel interaction method for 3D multi-object removal, enabling users to select regions and click on objects and background to retain in any given view, followed by the removal of the remaining objects. Considering that the mask correspondence across multiple views is a key challenge in multi-view object removal, we propose a novel end-to-end method based on warping and adaptive anchor circles. Specifically, we compute the homography matrix for mask warping with keypoints matching pairs between multi-view images, then adjust the size of the anchor circle using constraints from the segmentation mask and the warped mask. Furthermore, points are sampled from the anchor circle to serve as the SAM2 point prompts for each view, ultimately obtaining the final mask. Notably, our method does not require any depth or pose information, making it easier to apply to real-world scenarios. Experimental results on public datasets and our proposed dataset demonstrate the effectiveness and efficiency of our method. In future work, we will explore how to achieve high-quality 3D object removal relying solely on sparse viewpoint images.

References

- [Avrahami *et al.*, 2022] Omri Avrahami, Dani Lischinski, and Ohad Fried. Blended diffusion for text-driven editing of natural images. In *CVPR*, pages 18208–18218, 2022.
- [Avrahami *et al.*, 2023] Omri Avrahami, Ohad Fried, and Dani Lischinski. Blended latent diffusion. *ACM TOG*, 42(4):1–11, 2023.
- [Chen *et al.*, 2023] Jiaben Chen, Renrui Zhang, Dongze Lian, Jiaqi Yang, Ziyao Zeng, and Jianbo Shi. iquery: Instruments as queries for audio-visual sound separation. In *Proceedings of the IEEE/CVF Conference on Computer Vision and Pattern Recognition*, pages 14675–14686, 2023.
- [Chen *et al.*, 2024] Honghua Chen, Chen Change Loy, and Xingang Pan. Mvip-nerf: Multi-view 3d inpainting on nerf scenes via diffusion prior. In *CVPR*, pages 5344–5353, 2024.
- [Choy *et al.*, 2019] Christopher Choy, JunYoung Gwak, and Silvio Savarese. 4d spatio-temporal convnets: Minkowski convolutional neural networks. In *CVPR*, pages 3075–3084, 2019.
- [Dosovitskiy, 2020] Alexey Dosovitskiy. An image is worth 16x16 words: Transformers for image recognition at scale. *arXiv preprint arXiv:2010.11929*, 2020.
- [Genova *et al.*, 2021] Kyle Genova, Xiaoqi Yin, Abhijit Kundu, Caroline Pantofaru, Forrester Cole, Avneesh Sud, Brian Brewington, Brian Shucker, and Thomas Funkhouser. Learning 3d semantic segmentation with only 2d image supervision. In *3DV*, pages 361–372, 2021.
- [Gu and Dao, 2023] Albert Gu and Tri Dao. Mamba: Linear-time sequence modeling with selective state spaces. *arXiv preprint arXiv:2312.00752*, 2023.
- [Guo *et al.*, 2020] Yulan Guo, Hanyun Wang, Qingyong Hu, Hao Liu, Li Liu, and Mohammed Bennamoun. Deep learning for 3d point clouds: A survey. *IEEE TPAMI*, 43(12):4338–4364, 2020.
- [Ho *et al.*, 2020] Jonathan Ho, Ajay Jain, and Pieter Abbeel. Denoising diffusion probabilistic models. In *NeurIPS*, pages 6840–6851, 2020.
- [Hu *et al.*, 2021] Wenbo Hu, Hengshuang Zhao, Li Jiang, Jiaya Jia, and Tien-Tsin Wong. Bidirectional projection network for cross dimension scene understanding. In *CVPR*, pages 14373–14382, 2021.
- [Kirillov *et al.*, 2023] Alexander Kirillov, Eric Mintun, Nikhila Ravi, Hanzi Mao, Chloe Rolland, Laura Gustafson, Tete Xiao, Spencer Whitehead, Alexander C Berg, Wan-Yen Lo, et al. Segment anything. In *ICCV*, pages 4015–4026, 2023.
- [Li *et al.*, 2020] Jingyuan Li, Ning Wang, Lefei Zhang, Bo Du, and Dacheng Tao. Recurrent feature reasoning for image inpainting. In *CVPR*, pages 7760–7768, 2020.
- [Li *et al.*, 2022] Wenbo Li, Zhe Lin, Kun Zhou, Lu Qi, Yi Wang, and Jiaya Jia. Mat: Mask-aware transformer for large hole image inpainting. In *CVPR*, pages 10758–10768, 2022.
- [Lin *et al.*, 2024] Chieh Hubert Lin, Changil Kim, Jia-Bin Huang, Qinbo Li, Chih-Yao Ma, Johannes Kopf, Ming-Hsuan Yang, and Hung-Yu Tseng. Taming latent diffusion model for neural radiance field inpainting. In *ECCV*, 2024.
- [Lu *et al.*, 2024] Yiren Lu, Jing Ma, and Yu Yin. View-consistent object removal in radiance fields. In *ACM MM*, 2024.
- [Lugmayr *et al.*, 2022] Andreas Lugmayr, Martin Danelljan, Andres Romero, Fisher Yu, Radu Timofte, and Luc Van Gool. Repaint: Inpainting using denoising diffusion probabilistic models. In *CVPR*, pages 11461–11471, 2022.
- [Maturana and Scherer, 2015] Daniel Maturana and Sebastian Scherer. Voxnet: A 3d convolutional neural network for real-time object recognition. In *IROS*, pages 922–928, 2015.
- [Mildenhall *et al.*, 2021] Ben Mildenhall, Pratul P Srinivasan, Matthew Tancik, Jonathan T Barron, Ravi Ramamoorthi, and Ren Ng. Nerf: Representing scenes as neural radiance fields for view synthesis. *CACM*, 65(1):99–106, 2021.
- [Mirzaei *et al.*, 2023a] Ashkan Mirzaei, Tristan Aumentado-Armstrong, Marcus A Brubaker, Jonathan Kelly, Alex Levinshtein, Konstantinos G Derpanis, and Igor Gilitschenski. Reference-guided controllable inpainting of neural radiance fields. In *ICCV*, pages 17815–17825, 2023.
- [Mirzaei *et al.*, 2023b] Ashkan Mirzaei, Tristan Aumentado-Armstrong, Konstantinos G Derpanis, Jonathan Kelly, Marcus A Brubaker, Igor Gilitschenski, and Alex Levinshtein. Spin-nerf: Multiview segmentation and perceptual inpainting with neural radiance fields. In *CVPR*, pages 20669–20679, 2023.
- [Nichol *et al.*, 2021] Alex Nichol, Prafulla Dhariwal, Aditya Ramesh, Pranav Shyam, Pamela Mishkin, Bob McGrew, Ilya Sutskever, and Mark Chen. Glide: Towards photorealistic image generation and editing with text-guided diffusion models. *arXiv preprint arXiv:2112.10741*, 2021.
- [Pathak *et al.*, 2016] Deepak Pathak, Philipp Krahenbuhl, Jeff Donahue, Trevor Darrell, and Alexei A Efros. Context encoders: Feature learning by inpainting. In *CVPR*, pages 2536–2544, 2016.
- [Qi *et al.*, 2017a] Charles R. Qi, Hao Su, Kaichun Mo, and Leonidas J. Guibas. Pointnet: Deep learning on point sets for 3d classification and segmentation. In *CVPR*, pages 652–660, 2017.
- [Qi *et al.*, 2017b] Charles Ruizhongtai Qi, Li Yi, Hao Su, and Leonidas J Guibas. Pointnet++: Deep hierarchical feature learning on point sets in a metric space. In *NeurIPS*, pages 5099–5108, 2017.
- [Radford *et al.*, 2021] Alec Radford, Jong Wook Kim, Chris Hallacy, Aditya Ramesh, Gabriel Goh, Sandhini Agarwal, Girish Sastry, Amanda Askell, Pamela Mishkin, Jack Clark, et al. Learning transferable visual models from natural language supervision. In *ICML*, pages 8748–8763, 2021.

- [Ravi *et al.*, 2024] Nikhila Ravi, Valentin Gabeur, Yuan-Ting Hu, Ronghang Hu, Chaitanya Ryali, Tengyu Ma, Haitham Khedr, Roman Rädle, Chloe Rolland, Laura Gustafson, Eric Mintun, Junting Pan, Kalyan Vasudev Alwala, Nicolas Carion, Chao-Yuan Wu, Ross Girshick, Piotr Dollár, and Christoph Feichtenhofer. Sam 2: Segment anything in images and videos. *arXiv preprint arXiv:2408.00714*, 2024.
- [Ren *et al.*, 2019] Yurui Ren, Xiaoming Yu, Ruonan Zhang, Thomas H Li, Shan Liu, and Ge Li. Structureflow: Image inpainting via structure-aware appearance flow. In *ICCV*, pages 181–190, 2019.
- [Rombach *et al.*, 2022] Robin Rombach, Andreas Blattmann, Dominik Lorenz, Patrick Esser, and Björn Ommer. High-resolution image synthesis with latent diffusion models. In *CVPR*, pages 10684–10695, 2022.
- [Schönberger *et al.*, 2016] Johannes Lutz Schönberger, Enliang Zheng, Marc Pollefeys, and Jan-Michael Frahm. Pixelwise view selection for unstructured multi-view stereo. In *European Conference on Computer Vision (ECCV)*, 2016.
- [Shen *et al.*, 2024] Sitian Shen, Zilin Zhu, Linqian Fan, Harry Zhang, and Xinxiao Wu. Diffclip: Leveraging stable diffusion for language grounded 3d classification. In *WACV*, pages 3596–3605, 2024.
- [Sun *et al.*, 2021] Jiaming Sun, Zehong Shen, Yuang Wang, Hujun Bao, and Xiaowei Zhou. Loftr: Detector-free local feature matching with transformers. In *CVPR*, pages 8922–8931, 2021.
- [Suvorov *et al.*, 2022] Roman Suvorov, Elizaveta Logacheva, Anton Mashikhin, Anastasia Remizova, Arsenii Ashukha, Aleksei Silvestrov, Naejin Kong, Harshith Goka, Kiwoong Park, and Victor Lempitsky. Resolution-robust large mask inpainting with fourier convolutions. In *WACV*, pages 2149–2159, 2022.
- [Tancik *et al.*, 2023] Matthew Tancik, Ethan Weber, Evonne Ng, Ruilong Li, Brent Yi, Justin Kerr, Terrance Wang, Alexander Kristoffersen, Jake Austin, Kamyar Salahi, Abhik Ahuja, David McAllister, and Angjoo Kanazawa. Nerfstudio: A modular framework for neural radiance field development. In *ACM SIGGRAPH 2023 Conference Proceedings, SIGGRAPH '23*, 2023.
- [Vaswani *et al.*, 2017] Ashish Vaswani, Noam Shazeer, Niki Parmar, Jakob Uszkoreit, Llion Jones, Aidan N Gomez, Łukasz Kaiser, and Illia Polosukhin. Attention is all you need. In *NeurIPS*, 2017.
- [Wan *et al.*, 2021] Ziyu Wan, Jingbo Zhang, Dongdong Chen, and Jing Liao. High-fidelity pluralistic image completion with transformers. In *ICCV*, pages 4692–4701, 2021.
- [Wang *et al.*, 2024a] Dongqing Wang, Tong Zhang, Alaa Abboud, and Sabine Süsstrunk. Innerf360: Text-guided 3d-consistent object inpainting on 360-degree neural radiance fields. In *CVPR*, pages 12677–12686, 2024.
- [Wang *et al.*, 2024b] Yuxin Wang, Qianyi Wu, Guofeng Zhang, and Dan Xu. Gstream: Learning 3d geometry and feature consistent gaussian splatting for object removal. In *ECCV*, 2024.
- [Weber *et al.*, 2024] Ethan Weber, Aleksander Holynski, Varun Jampani, Saurabh Saxena, Noah Snavely, Abhishek Kar, and Angjoo Kanazawa. Nerfiller: Completing scenes via generative 3d inpainting. In *CVPR*, pages 20731–20741, 2024.
- [Weder *et al.*, 2023] Silvan Weder, Guillermo Garcia-Hernando, Aron Monszpart, Marc Pollefeys, Gabriel J Brostow, Michael Firman, and Sara Vicente. Removing objects from neural radiance fields. In *CVPR*, pages 16528–16538, 2023.
- [Wei *et al.*, 2023] Fangyin Wei, Thomas Funkhouser, and Szymon Rusinkiewicz. Clutter detection and removal in 3d scenes with view-consistent inpainting. In *ICCV*, pages 18131–18141, 2023.
- [Wu *et al.*, 2022] Xiaoyang Wu, Yixing Lao, Li Jiang, Xihui Liu, and Hengshuang Zhao. Point transformer v2: Grouped vector attention and partition-based pooling. In *NeurIPS*, pages 33330–33342, 2022.
- [Wu *et al.*, 2024] Xiaoyang Wu, Li Jiang, Peng-Shuai Wang, Zhijian Liu, Xihui Liu, Yu Qiao, Wanli Ouyang, Tong He, and Hengshuang Zhao. Point transformer v3: Simpler, faster, stronger. In *CVPR*, pages 4840–4851, 2024.
- [Xie *et al.*, 2023] Shaoan Xie, Zhifei Zhang, Zhe Lin, Tobias Hinz, and Kun Zhang. Smartbrush: Text and shape guided object inpainting with diffusion model. In *CVPR*, pages 22428–22437, 2023.
- [Yang *et al.*, 2023] Cheng-Kun Yang, Min-Hung Chen, Yung-Yu Chuang, and Yen-Yu Lin. 2d-3d interlaced transformer for point cloud segmentation with scene-level supervision. In *ICCV*, pages 977–987, 2023.
- [Yang *et al.*, 2024a] Fengyu Yang, Chao Feng, Ziyang Chen, Hyoungeob Park, Daniel Wang, Yiming Dou, Ziyao Zeng, Xien Chen, Rit Gangopadhyay, Andrew Owens, et al. Binding touch to everything: Learning unified multimodal tactile representations. In *CVPR*, pages 26340–26353, 2024.
- [Yang *et al.*, 2024b] Fengyu Yang, Chao Feng, Daniel Wang, Tianye Wang, Ziyao Zeng, Zhiyang Xu, Hyoungeob Park, Pengliang Ji, Hanbin Zhao, Yuanning Li, et al. Neurobind: Towards unified multimodal representations for neural signals. *arXiv preprint arXiv:2407.14020*, 2024.
- [Yu *et al.*, 2019] Jiahui Yu, Zhe Lin, Jimei Yang, Xiaohui Shen, Xin Lu, and Thomas S Huang. Free-form image inpainting with gated convolution. In *ICCV*, pages 4471–4480, 2019.
- [Zeng *et al.*, 2024a] Ziyao Zeng, Jingcheng Ni, Daniel Wang, Patrick Rim, Younjoon Chung, Fengyu Yang, Byung-Woo Hong, and Alex Wong. Priordiffusion: Leverage language prior in diffusion models for monocular depth estimation. *arXiv preprint arXiv:2411.16750*, 2024.

- [Zeng *et al.*, 2024b] Ziyao Zeng, Daniel Wang, Fengyu Yang, Hyoungseob Park, Stefano Soatto, Dong Lao, and Alex Wong. Worddepth: Variational language prior for monocular depth estimation. In *Proceedings of the IEEE/CVF Conference on Computer Vision and Pattern Recognition*, pages 9708–9719, 2024.
- [Zeng *et al.*, 2024c] Ziyao Zeng, Yangchao Wu, Hyoungseob Park, Daniel Wang, Fengyu Yang, Stefano Soatto, Dong Lao, Byung-Woo Hong, and Alex Wong. Rsa: Resolving scale ambiguities in monocular depth estimators through language descriptions. *arXiv preprint arXiv:2410.02924*, 2024.
- [Zhang *et al.*, 2018] Haoran Zhang, Zhenzhen Hu, Changzhi Luo, Wangmeng Zuo, and Meng Wang. Semantic image inpainting with progressive generative networks. In *ACM MM*, pages 1939–1947, 2018.
- [Zhang *et al.*, 2021] Renrui Zhang, Ziyao Zeng, Ziyu Guo, Xinben Gao, Kexue Fu, and Jianbo Shi. Dspoint: Dual-scale point cloud recognition with high-frequency fusion. *arXiv preprint arXiv:2111.10332*, 2021.
- [Zhang *et al.*, 2022a] Renrui Zhang, Ziyu Guo, Wei Zhang, Kunchang Li, Xupeng Miao, Bin Cui, Yu Qiao, Peng Gao, and Hongsheng Li. Pointclip: Point cloud understanding by CLIP. In *CVPR*, pages 8542–8552, 2022.
- [Zhang *et al.*, 2022b] Renrui Zhang, Ziyao Zeng, Ziyu Guo, and Yafeng Li. Can language understand depth? In *Proceedings of the 30th ACM International Conference on Multimedia*, pages 6868–6874, 2022.
- [Zhao *et al.*, 2023] Weiguang Zhao, Yuyao Yan, Chaolong Yang, Jianan Ye, Xi Yang, and Kaizhu Huang. Divide and conquer: 3d point cloud instance segmentation with point-wise binarization. In *ICCV*, pages 562–571, 2023.
- [Zhao *et al.*, 2025] Weiguang Zhao, Guanyu Yang, Rui Zhang, Chenru Jiang, Chaolong Yang, Yuyao Yan, Amir Hussain, and Kaizhu Huang. Open-pose 3d zero-shot learning: Benchmark and challenges. *NN*, 181:106775, 2025.
- [Zheng *et al.*, 2019] Chuanxia Zheng, Tat-Jen Cham, and Jianfei Cai. Pluralistic image completion. In *CVPR*, pages 1438–1447, 2019.
- [Zhu *et al.*, 2023a] Xiangyang Zhu, Renrui Zhang, Bowei He, Ziyu Guo, Ziyao Zeng, Zipeng Qin, Shanghang Zhang, and Peng Gao. Pointclip v2: Prompting clip and gpt for powerful 3d open-world learning. In *Proceedings of the IEEE/CVF International Conference on Computer Vision*, pages 2639–2650, 2023.
- [Zhu *et al.*, 2023b] Xiangyang Zhu, Renrui Zhang, Bowei He, Ziyu Guo, Ziyao Zeng, Zipeng Qin, Shanghang Zhang, and Peng Gao. Pointclip v2: Prompting clip and gpt for powerful 3d open-world learning. In *ICCV*, pages 2639–2650, 2023.